Sterling J. Anderson,
Sisir B. Karumanchi,
and Karl Iagnemma
Department of Mechanical Engineering
Massachusetts Institute of Technology
Cambridge, MA, USA
E-mails: ster@mit.edu, sisir@mit.edu, and kdi@mit.edu

James M. Walker
Quantum Signal, LLC
Saline, MI, USA
E-mail: jwalker@quantumsignal.com

The Intelligent CoPilot

A Constraint-Based Approach to Shared-Adaptive Control of Ground Vehicles

***Abstract*—This paper presents a new approach to semi-autonomous vehicle hazard avoidance and stability control, based on the design and selective enforcement of constraints. This differs from traditional approaches that rely on the planning and tracking of paths and facilitates "minimally-invasive" control for human-machine systems. Instead of forcing a human operator to follow an automation-determined path, the constraint-based approach identifies safe homotopies, and allows the operator to navigate freely within them, introducing control action only as necessary to ensure that the vehicle does not violate safety constraints. This method evaluates candidate homotopies based on "restrictiveness," rather than traditional measures of path goodness, and designs and enforces requisite constraints on the human's control commands to ensure that the vehicle never leaves the controllable subset of a desired homotopy. This paper demonstrates the approach in simulation and characterizes its effect on human teleoperation of unmanned ground vehicles via a 20-user, 600-trial study on an outdoor obstacle course. Aggregated across all drivers and experiments, the constraint-based control system required an average of 43% of the available control authority to reduce collision frequency by 78% relative to traditional teleoperation, increase average speed by 26%, and moderate operator steering commands by 34%.**

I. Introduction

Humans make mistakes. When humans control dynamic systems, the rate and ramifications of those mistakes increase. Whether it occurs while driving a car, controlling industrial machinery, or teleoperating an unmanned vehicle, human error can lead to costly and often deadly consequences. In 2010, over 32,000 people were killed and another 2.2 million injured in motor vehicle accidents in the United States alone [1]. The U.S. military is also strongly affected by human error, with vehicle crashes representing the leading cause of non-hostile deaths in Operation Iraqi Freedom [2]. Even unmanned ground vehicles are susceptible, as operators must not only cope with the challenges inherent to the manned driving task, but must perform many of the same functions with a restricted field of view, limited depth perception, potentially disorienting camera viewpoints,

Digital Object Identifier 10.1109/MITS.2013.2247796
Date of publication: 23 April 2013

1939-1390/13/$31.00©2013IEEE

and significant time delays [3]. Remotely operating a ground vehicle under these conditions while monitoring the vehicle's health status, the status of the mission/tasks, and the condition of the environment leads to high failure rates [4].

Semi-autonomous control offers a unique opportunity to improve human performance through the exploitation of human-automation synergies. As originally published in 1951 [5] and widely discussed since, humans and automation are uniquely well suited to specific types of tasks [6]. Whereas automation excels at responding quickly and precisely to well-defined or repetitive control objectives, humans tend to make more mistakes as the frequency and complexity of the control task increase. Conversely, humans have the unique ability to detect and contextualize patterns and new information, reason inductively, and adapt to new modes of operation, whereas automation typically struggles at these tasks. The goal of semi-autonomy is to exploit synergies in the abilities of humans and automation to improve planning and control performance of the combined system and—where possible—the actors therein.

A. Previous Work

Research to date in vehicle control has left a significant gap between fully-autonomous planning and control frameworks, which neither account for nor provide an effective means of cooperating with the human operator, and driver assistance systems which are typically limited to local, one-dimensional support. While these classes of system are distinct in their intended outcomes, their inability to effectively share control with a human driver has its root in a common, basic building block: each relies on specific, planned paths.

In the context of autonomous control, many methods exist for planning paths. Common path planning tools include rapidly-exploring random trees [7], graph search methods [8], potential fields [9], and neural optimization techniques [10]. Control laws routinely used to track these reference paths include PID schemes, linear-quadratic regulators, and nonlinear fuzzy controllers. While many variations of this planning-then-control approach have proven effective in autonomous implementations [11], their reliance on a specific reference path (which is in many cases arbitrary, non-intuitive, and over-restrictive to a human operator), and consequent inability to account for the planning preferences and control inputs of a human operator make them ill-suited for human-in-the-loop or "semi-autonomous" control.

At the other end of the vehicle safety community, with an eye on nearer-term, industry-driven objectives, researchers have developed systems that assist the human operator in avoiding collisions and loss of stability. These active safety systems traditionally fall into one of two categories: reactive safety systems, such as antilock brakes, traction controllers, electronic stability controllers, and lane-assist approaches monitor the current state of the vehicle and apply low-level control actions to meet some safety-critical criteria [12]. For example, stability controllers monitor the lateral acceleration, yaw, and wheel rotational speeds, and apply asymmetric torques to the wheels when estimated lateral or longitudinal tire slip exceeds a prespecified threshold. In order to avoid collisions, these systems rely on the human's ability to 1) foresee, 2) judge, and 3) respond appropriately to impending hazards to trigger intervention. This reliance on driver actions renders reactive safety systems vulnerable to human recognition and decision errors; for drivers who do not recognize and correctly respond to hazards, these systems can do very little.

Predictive safety systems consider not only the current state of the vehicle, but also its predicted state evolution and that of environmental hazards. These systems then preemptively assist the driver in identifying, assessing the threat posed by, and in some cases avoiding an impending hazard. Recent work in predictive safety has resulted in systems that use audible warnings [13], haptic alerts [14] and steering torque overlays [15] to help the driver avoid collisions [16], instability [17], or lane departure [18]. Similar to autonomous systems, the path-based prediction metrics used by these systems limits their ability to provide more than local, one-dimensional support. For instance, lane-keeping systems monitor only the lateral position of the vehicle relative to lane markings and provide driver warnings, additional steering torque, or differential brake pressure to assist the driver in laterally positioning the vehicle [18]. Similarly, adaptive cruise control systems regulate only the longitudinal position and closing speed of the ego vehicle relative to a preceding vehicle [19].

Between the strategic, multidimensional capabilities of autonomous planning and control systems and the more tactical, one-dimensional focus of driver-assistance systems lies a significant need for planning and control techniques capable of both strategic planning and intuitive, "intention-preserving" control support. We posit that such a system should be designed to accommodate the constraint-based planning and control technique humans have long been shown to exhibit [20]. Rather than obsessively planning and tracking a single path, humans tend instead to identify a field of safe travel—one that contains an infinite number of continuously deformable ("homotopic") paths—and control the vehicle within it. This homotopy selection arguably represents the highest level of human reasoning employed in the navigation task and reduces the subsequent burden of calculating and applying appropriate control inputs to that of simply remaining within the desired homotopy.

On an open roadway, for example, the preferred homotopy often contains many acceptable paths traversing a desired lane. In off-road environments, the desired homotopy may not be as clearly delineated, though vehicle dynamic constraints require that it exclude any region through which the vehicle cannot travel without colliding with obstacle(s). Figure 1 illustrates three prominent

homotopies in a cluttered environment as they might be perceived by a human operator.

Instead of planning a path and restricting the human operator to that path, we propose a constraint-based semi-autonomous system that strategically limits the range of available inputs to ensure that the operator retains as much control freedom as possible without risking collision with obstacles or dynamic instability.

B. Paper Outline

This paper introduces a new approach to semi-autonomous control; one in which homotopies and their associated constraints are identified, characterized, planned, and enforced to ensure that the controlled system (an off-road ground vehicle in this case) avoids hazards and loss of stability without unduly restricting the control freedom of a human operator. Section II describes the methods used to plan and characterize constraints on the vehicle position. Section III then describes one method for converting those constraints into semi-autonomously enforceable constraints on the operator's control commands. These methods are demonstrated in control of a simulated ground vehicle through an obstacle field (Section IV) and semi-autonomous teleoperation of a Kawasaki Mule through a similar field (Section V). The paper then closes with general conclusions.

II. Constraint Planning

Planning in constraint or "homotopy space" requires the identification of homotopies and an evaluation of their goodness. Because the constraints bounding a homotopy admit an infinite number of paths, identifying and evaluating the "goodness" of these constraints requires a new set of evaluation criterion from those commonly used in path planning. Whereas the goodness or "optimality" of a specific path is well defined using metrics such as length, curvature, and dynamic feasibility, corresponding measures lose their traditional meaning when applied to a set of constraints and the many paths they admit. Further, planning methods typically used to design paths, such as graph search, potential fields, and sampling-based algorithms, will not necessarily work to plan constraints since the latter must be designed to circumscribe—rather than simply remain within—a safe operating region. In light of this inherent difficulty, a method is presented here based on the constrained Delaunay triangulation, which provides a useful physical boundary to, and heuristic evaluation of, the many distinct paths existing within a given homotopy.

A. Homotopy Identification

As illustrated in Figure 1, any environment bifurcated by obstacles or impassible regions admits multiple path homotopies. A path homotopy is a set of paths that can be continuously deformed into one another without crossing infeasible regions. If a particular homotopy can be identified, vehicle position constraints may be designed at its edges to circumscribe the set of paths it contains and thereby ensure that the vehicle remains safely within it (avoiding collisions with obstacles).

FIG 1 Visualization of prominent homotopies available to a human operator (image best viewed in color).

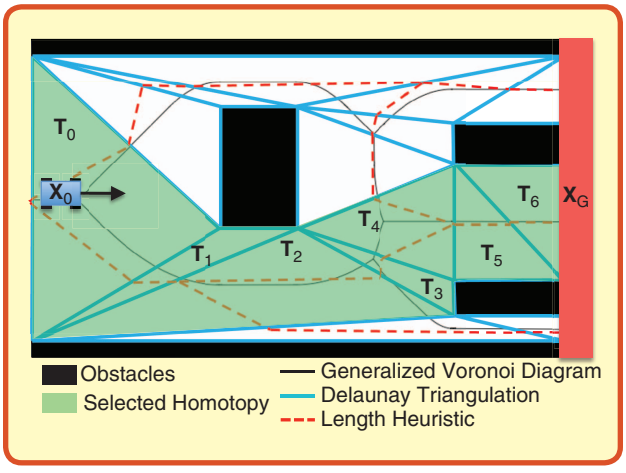

FIG 2 Illustration of triangulated environment showing homotopy selection and dual graph for length heuristic.

In this work, we identify homotopies by decomposing a two-dimensional configuration space $\mathbf{C} \in \mathbf{R}^2$ containing convex, polygonal obstacles[1] into a complete set of constrained Delaunay triangles. The dual graph of this triangulation provides a search space through which homotopies may be planned via standard graph search methods. That is, any feasible homotopy containing the vehicle's current position $\mathbf{X_0}$, and the position of the goal location, $\mathbf{X_G}$, may be defined as a sequence $\boldsymbol{H^n}$ of adjacent triangles $\mathbf{T_0} \ldots \mathbf{T_n}$ extending from the triangle circumscribing the vehicle's current position ($\mathbf{T_0}$ in Figure 2) to that containing the goal location(s). This goal may be described by a single point or by a region of $\mathbf{R^2}$, such as the distal edge of the local sensing window illustrated in red in Figure 2.

B. Homotopy Evaluation

In order to plan a set of constraints circumscribing a desired homotopy, metrics describing homotopy goodness must be defined and ascribed to individual triangles and

[1]Methods for convexifying non-convex polygons described in [21], [22].

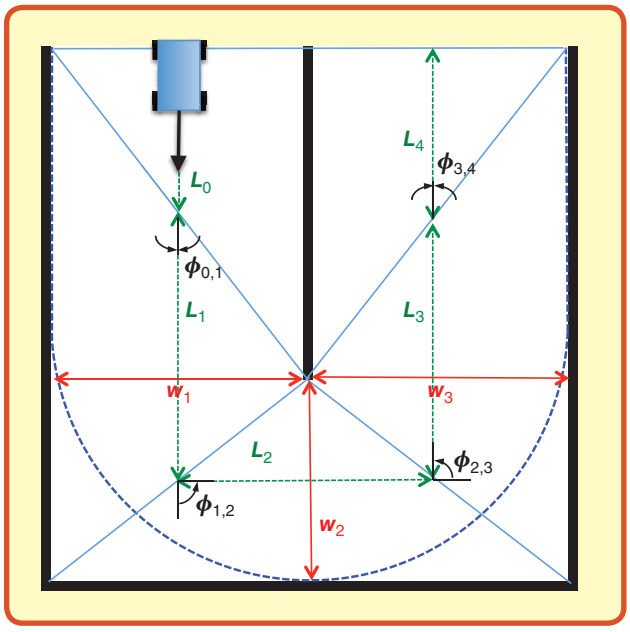

FIG 3 Illustration of a triangulated channel and the heuristics used to describe constraint restrictiveness and dynamic feasibility.

transitions between them. We here propose geometric and reachability heuristics for evaluating homotopy goodness. These include an estimate of the average distance traveled by paths within it, an estimate of the control freedom it affords an operator, and an approximation of its dynamic reachability given the vehicle's current state.

Given a constrained Delaunay triangulation of C, we note that any path belonging to a particular homotopy $\mathbf{H}^n = \mathbf{T}_0 \cup \mathbf{T}_1 \cup \ldots \cup \mathbf{T}_n$ will pass through each triangle $\mathbf{T}_k$ in $\mathbf{H}^n$ at least once. A path enters $\mathbf{T}_k$ through the edge it shares with $\mathbf{T}_{k-1}(\mathbf{E}_{k-1,k})$ and exits through $\mathbf{E}_{k,k+1}$ into $\mathbf{T}_{k+1}$. Thus, the average "distance" traveled by all triangle-monotonic (passing through each edge at most once) paths belonging to a given homotopy as it crosses $\mathbf{T}_k$ may be heuristically described as the distance from the midpoint of $\mathbf{E}_{k-1,k}$ to that of $\mathbf{E}_{k,k+1}$. As Figure 2 illustrates, the dual graph embodying this heuristic closely resembles the Generalized Voronoi Diagram (GVD).

While the average "length" of paths belonging to a particular homotopy may be described by the distance metric above, the "restrictiveness" and dynamic feasibility of the constraints bounding this homotopy require heuristic evaluations of the range of motion and control freedom they admit. To incorporate these considerations into the constraint-planning problem, we observe the following:

1) The dynamic feasibility of any path followed by a vehicle with Dubins constraints and friction-limited tires may be characterized by the lateral acceleration it requires.
2) This lateral acceleration is directly proportional to the square of vehicle velocity and inversely proportional to the radius of curvature of the path it follows.
3) In any homotopy $\mathbf{H}^n$, the maximum radius of curvature of any of the constant-velocity paths belonging to $\mathbf{H}^n$ is limited by the "width" $\boldsymbol{w}_k$, or minimum pass-through clearance of the Delaunay Triangles comprising the homotopy. As illustrated in Figure 3, $\boldsymbol{w}_k$ is calculated as the perpendicular distance from the constrained edge of the triangle to the apex opposite the constrained edge. If $\mathbf{T}_k$ is obtuse and either $\mathbf{E}_{k-1,k}$ or $\mathbf{E}_{k,k+1}$ lie opposite the obtuse vertex, $\boldsymbol{w}_k$ is instead calculated as the shorter of $\mathbf{E}_{k-1,k}$ and $\mathbf{E}_{k,k+1}$. The blue dashed line in Figure 3 illustrates the maximal radius path belonging to a particular homotopy.
4) This maximal curvature is also affected by the relative orientation of adjacent constrained edges, or equivalently, the difference in orientation $\boldsymbol{\phi}_{k-1,k}$ for adjacent line segments $\boldsymbol{L}_{k-1}$ and $\boldsymbol{L}_k$ of the dual graph used to calculate "length" (these being parallel to the constrained edge).

Finally, while the above heuristics give an estimate of the dynamic feasibility of a set of constraints, they do not explicitly account for the dynamic reachability of the homotopy itself from the vehicle's current state. This consideration is incorporated into the homotopy planning layer using an adaptation of the dynamic window approach originally described in [23]. Rather than map obstacles onto a 2-dimensional velocity search space, however, our approach instead maps the total vehicle acceleration required to avoid obstacles onto the one-dimensional steering space of the vehicle. It then calculates the surplus tire friction available to the human driver if s/he were to steer into either homotopy. Steering angles from which the vehicle cannot avoid a collision with an impending obstacle are excluded from this area calculation. Figure 4(b) illustrates one such region (labeled "Collision Imminent") corresponding to a range of steering angles from within which the vehicle cannot avoid the black obstacle at its current speed. Regions A_m and A_n correspond to the surplus acceleration available by crossing edges $E_{1,m}$, and $E_{1,n}$, respectively.

Assuming constant velocity V, wheelbase length L, tire friction coefficient μ, gravity g, stationary obstacles, and no-slip conditions, the minimal avoidance acceleration required to avoid obstacle • is given by

$$a_{\bullet}(\delta) = \begin{cases} 0 & \delta \le \delta_{\bullet,1} \\ \frac{1}{2}\sqrt{\frac{V^4 \tan\delta (4\phi^2+1)}{L^2\phi^2}} & \delta_{\bullet,1} \le \delta \le \delta_{\bullet,2} \\ 0 & \delta_{\bullet,2} \le \delta, \end{cases} \quad (1)$$

where

$$\phi = \arctan\left(\frac{x\tan\delta}{L - y\tan\delta}\right), \quad (2)$$

and

$$\delta = \arctan\left(\frac{2Ly}{x^2+y^2}\right). \quad (3)$$

Summed over the steering angles corresponding to the homotopy choices, the surplus tire friction for homotopy i is then given by

$$\alpha^i_{\text{sur}} = \int_{\Delta^i_{\min}}^{\Delta^i_{\max}} [\mu g - \max(\{a_j(\delta): j = 1,\ldots,n\})]d\delta$$
$$\Delta^i_{\max} = \min(\delta^{\max}_{\text{actuator}}, \delta^{\max}_{\text{kinematic}}, \max(\delta_{E_{1,m}}(1), \delta_{E_{1,n}}(2)))$$
$$\Delta^i_{\min} = \max(-\delta^{\min}_{\text{actuator}}, -\delta^{\min}_{\text{kinematic}}, \min(\delta_{E_{1,m}}(1), \delta_{E_{1,n}}(2))), \quad (4)$$

where $\delta_{E1,\cdot}(1)$ and $\delta_{E1,\cdot}(2)$ are the extremal steering angles reaching the two ends of edge $\mathbf{E}_{1,\cdot}$ (edges of the "Collision Steer" regions illustrated in Figure 4), $\delta^{\cdot}_{\text{actuator}}$ refers to physical steering limits, and $\delta^{\cdot}_{\text{kinematic}}$ represents the maximum non-slip steering angle allowed by the tire friction and current vehicle velocity ($\delta^{\cdot}_{\text{kinematic}} = \pm \arctan(\mu mgL/V^2)$).

With heuristics $\boldsymbol{L_k}, \boldsymbol{w_k}, \boldsymbol{\phi_k}$, and a^*_{surplus} thus calculated, a graph search (Dijkstra's algorithm is used here) may be performed to calculate the optimal path homotopy (a "channel" made of adjacent triangles) and its associated constraints. In the results shown in this paper, the objective function is defined as

$$\min_{T_i \ldots T_n} \left\{ k_{DW} \frac{1}{\alpha^i_{\text{sur}}} + \sum_{i=0}^{n} (k_L(L_{i-1,i}) + k_w \frac{1}{\min(w_{i-1}, w_i)} + k_\phi \mid \phi_{i-1,i} \mid) \right\} \quad (5)$$

$$\text{s.t.} \quad \begin{matrix} X_G \subseteq T_G \\ E_k = \{(T_k, T_{k+1})\} \end{matrix} \quad \text{where } E_k \text{ is unconstrained.} \quad (6)$$

This objective function incorporates an estimate of average homotopy "length" with an approximation of the control freedom and dynamic stability available to the vehicle as it traverses the homotopy. Weights $k_\cdot$ are tuned to reflect navigation priorities.

III. Constraint Enforcement

In the previous section, an objective function was defined to assess the goodness of a given homotopy. Once a desired homotopy has been identified, vehicle position constraints circumscribing the homotopy must be converted into semi-autonomously enforceable constraints on the human operator's control inputs as the vehicle traverses the constrained region.

To calculate these limits, a finite-horizon model predictive (MPC) controller is used to predict the vehicle state evolution within the desired homotopy under a stability-optimal control input sequence. The nearness of the predicted trajectory to stability limits is then used to compute the steering constraint applied at the vehicle and the torque feedback provided to the operator. These steps are briefly described below.

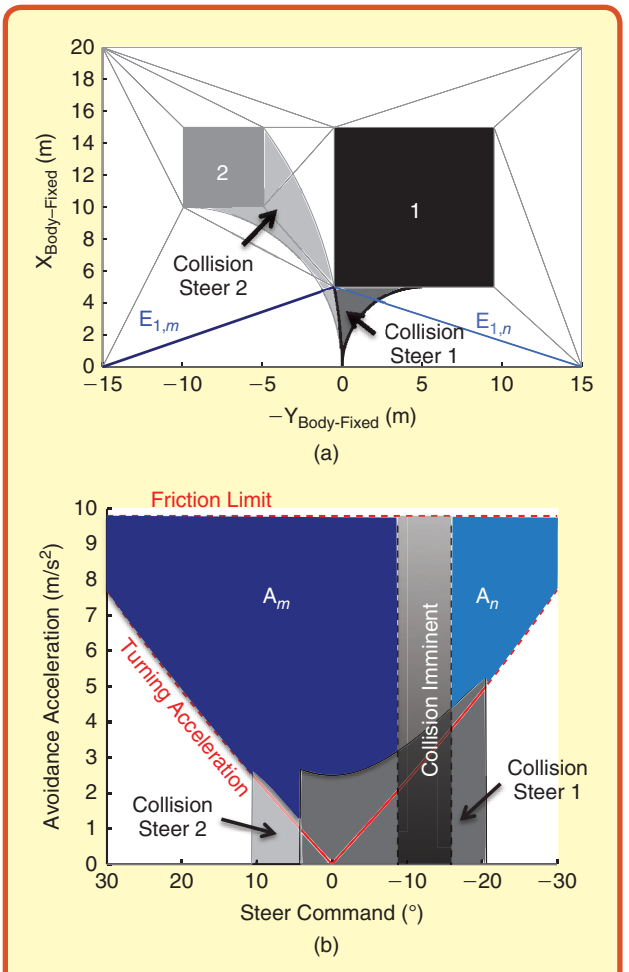

FIG 4 Illustration showing (a) triangularized environment with obstacles (gray and black), and (b) avoidance acceleration mapped to steering commands [with gray and black blocks corresponding to obstacles in (a)].

The MPC controller bases its predictions on a 4-wheeled vehicle model with slip and yaw dynamics. Defining vehicle states, outputs, inputs, and disturbances by $\mathbf{x}$, $\mathbf{y}$, $\mathbf{u}$, and $\mathbf{v}$, respectively, discrete plant dynamics are described by

$$\mathbf{x}_{k+1} = \mathbf{A}\mathbf{x}_k + \mathbf{B}_u\mathbf{u}_k + \mathbf{B}_v\mathbf{v}_k \quad (7)$$
$$\mathbf{y}_k = \mathbf{C}\mathbf{x}_k + \mathbf{D}_v\mathbf{v}_k. \quad (8)$$

A quadratic objective function over a prediction horizon of p sampling intervals is defined as

$$J_k = \sum_{i=k+1}^{k+p} \frac{1}{2}\mathbf{y}_i^T\mathbf{R}_y\mathbf{y}_i + \sum_{i=k}^{k+p-1} \frac{1}{2}\mathbf{u}_i^T\mathbf{R}_u\mathbf{u}_i + \sum_{i=k}^{k+p-1} \frac{1}{2}\Delta\mathbf{u}_i^T\mathbf{R}_{\Delta u}\Delta\mathbf{u}_i + \frac{1}{2}\rho_\varepsilon\varepsilon^2, \quad (9)$$

where $\mathbf{R}_y$, $\mathbf{R}_u$, and $\mathbf{R}_{\Delta u}$ represent diagonal weighting matrices penalizing deviations from $\mathbf{y_i} = \mathbf{u_i} = \Delta\mathbf{u_i} = 0$, ρ_ε represents the penalty on constraint violations, n denotes

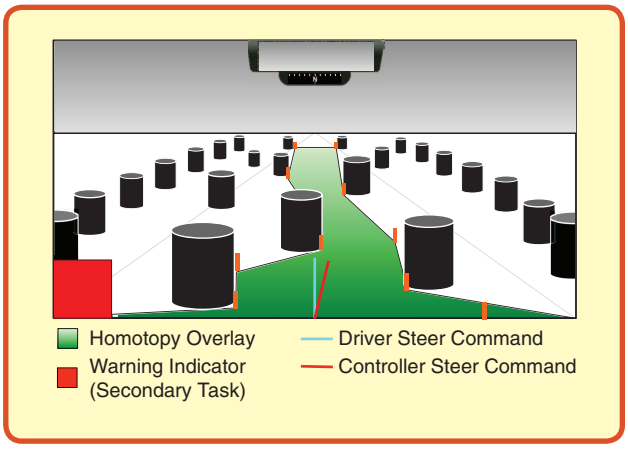

FIG 5 Illustration of the operator control interface.

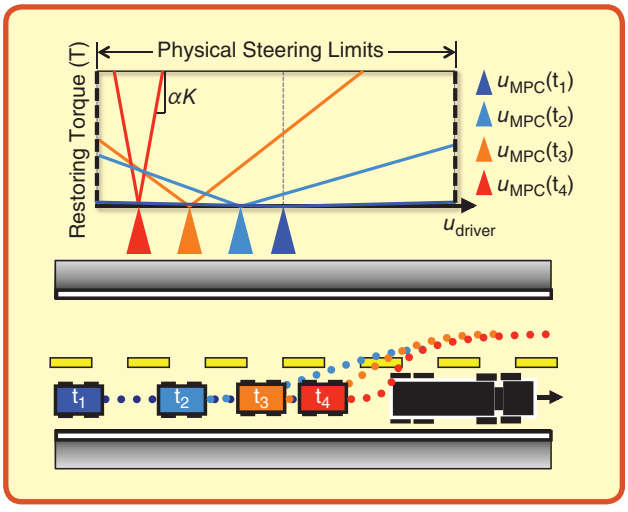

FIG 6 Scenario illustration showing the response of the restoring torque function as a vehicle successively approaches a hazard from behind.

the number of free control moves, and ε represents the maximum constraint violation over the prediction horizon p. Inequality constraints on vehicle position ($\mathbf{y}$), inputs ($\mathbf{u}$), and input rates ($\Delta\mathbf{u}$) are then defined as

$$\begin{aligned}\mathbf{y}^j_{\min}(i) - \varepsilon\mathbf{V}^j_{\min}(i) &\le \mathbf{y}^j(k+i+1|k)\\ &\le \mathbf{y}^j_{\max}(i) + \varepsilon\mathbf{V}^j_{\max}(i)\\ \mathbf{u}^j_{\min}(i) &\le \mathbf{u}^j(k+i+1|k) \le \mathbf{u}^j_{\max}(i)\\ \Delta\mathbf{u}^j_{\min}(i) &\le \Delta\mathbf{u}^j(k+i+1|k) \le \Delta\mathbf{u}^j_{\max}(i)\\ i &= 0,\ldots,p-1\\ \varepsilon &\ge 0,\end{aligned} \tag{10}$$

where the vector $\Delta\mathbf{u}$ represents the change in input from one sampling instant to the next, the superscript "$(\cdot)^j$" represents the jth component of a vector, k represents the current time, and the notation $(\cdot)^j(k+i\,|\,k)$ denotes the value predicted for time $k+i$ based on the information available at time k. The vector $\mathbf{V}$ allows for variable constraint softening over the prediction horizon, p, when ε is included in the objective function. The vectors $\mathbf{y}^y{}_{\min}$ and $\mathbf{y}^y{}_{\max}$ are sampled from the edges of the constrained channel $\mathbf{H}^n$. Also note that input constraints enforced in the MPC calculation are simply those imposed by available actuation.

The state trajectory $\overline{x}$ predicted by the MPC solution represents the state evolution of maximum stability that can be achieved given the vehicle's current position, dynamics, and homotopy constraints (imposed by $\mathbf{H}^n$). As such, the nearness of this prediction's stability-critical states to their physical limits provides a useful indication of the need for intervention and a natural boundary for the current vehicle control input.

Here, we define by "threat", Φ, the maximum predicted value of a stability-critical state (front wheel sideslip in this case). We then adjust the steering command seen by the vehicle (u_{vehicle}) to a blended sum of the optimal (u_{MPC}) and driver (u_{driver}) steering commands

$$u_{\text{vehicle}} = K(\Phi)u_{\text{MPC}} + (1 - K(\Phi))u_{\text{driver}}, \tag{11}$$

where $K \in [0\ \ 1]$ is computed using a piecewise linear function

$$K = \begin{cases} 0 & 0 \le \Phi \le \Phi_{\text{eng}} \\ \dfrac{\Phi - \Phi_{\text{eng}}}{\Phi_{\text{aut}} - \Phi_{\text{eng}}} & \Phi_{\text{eng}} \le \Phi \le \Phi_{\text{aut}} \\ 1 & \Phi \ge \Phi_{\text{aut}}. \end{cases} \tag{12}$$

Below a configurable threshold Φ_{eng}, $K = 0$ and the driver retains full control authority. Above Φ_{aut}, $K = 1$, and the MPC controller operates autonomously to satisfy state and homotopy constraints. Between Φ_{eng} and Φ_{aut}, control authority is shared.

This intervention ensures that at low threat, the vehicle closely matches operator commands while at high threat—when the safest maneuver satisfying homotopy constraints approaches the limit of vehicle stability—the vehicle steering command tracks the optimal command predicted by the MPC controller. For a complete treatment of this threat assessment and shared control method, the reader is referred to the authors' previous work [24].

In addition to constraints imposed on (or adjustments made to) the vehicle steering (which is transparent to the human operator), experimental tests also fed back a visual representation of the safe homotopy and a tactile set of "soft" constraints on the position of the steering wheel. This feedback was provided to improve the human operator's telepresence and situational awareness by indicating not only where the input constraints lie, but also how urgently they must be satisfied in order to avoid collision or loss of control.

Visual feedback was provided by overlaying a visual representation of the desired homotopy on the driver's screen as illustrated in Figure 5. In addition to the homotopy overlay,

steering angle indicators were provided at the bottom of the screen to show the driver where the vehicle is currently steering (red line), and where the driver's steering command lies relative to the vehicle's current steering angle. Section V.A describes the warning indicator.

> If the optimal steering command is expected to avoid both the hazard and loss of control, the controller exerts the maximum available torque on the operator's steering wheel.

The resistance torque applied to the operator's steering wheel is calculated as

$$\mathrm{T} = k_{\max} K \left| \delta_{\text{driver}} - \delta_{\text{MPC}} \right|, \tag{13}$$

where $k_{\max}$ represents the maximum available steering wheel torque and is used to re-dimensionalize K. Figure 6 illustrates the (hypothetical) response of the torque restoring function to increasingly threatening MPC predictions (assuming the driver fails to steer).

Notice that as time progresses (denoted by t_i labels on the host vehicle), the threat posed by the optimal maneuver prediction increases. Additionally, the immediate steering command required to track this optimal trajectory begins to drift leftward. The combined effect of an increasingly-urgent, and progressively-leftward u_{MPC} recommendation increases k_s and shifts the torque resistance trough. In the limiting case for which only the optimal steering command can reasonably be expected to avoid both the hazard and loss of control (sometime shortly after t_4), the controller exerts the maximum available torque on the operator's steering wheel, essentially ensuring that the operator not only cedes to the requirements of the controller, but is also aware of exactly what steering action is being taken by the vehicle.

IV. Simulation Testing

The constraint-based semi-autonomous controller was simulated using a nonlinear ADAMS model of a generic light truck. The MPC controller ran at 20 Hz. Its prediction and control horizons were calculated over 60 and 40 time steps, respectively. Parameters in the MPC model were configured to closely match those of the ADAMS plant, vehicle velocity was set at a constant 20 m/s, and simulated driver steering input was set to 0 degrees for generality. Figure 7 shows the path homotopy and associated position constraints designed by the path planner (green channel) as well as the control constraint imposed on the vehicle steering input (colorbar). Note that given the vehicle's initial position at (0,-2) [m], a shortest-path homotopy would have passed under the obstacles. Because this path is more tortuous and offers less control freedom to the human operator, the objective function described in (5) instead chooses the wider and less dynamically-challenging homotopy passing above the obstacles. Input constraints are initially tight in order to avoid the impending hazard, but quickly relax as the vehicle enters a less restricted region of the homotopy above the obstacles. Finally, we note that the "ricochet" off the upper obstacle occurs because the simulated "human" input remains at zero for the entire maneuver. In practice, the significant control freedom afforded by the relaxed constraints between x = 40 and 80 meters allows the human operator to straighten out of desired.

V. Experimental Testing

The effect of constraint-based semi-autonomy and driver feedback on driver performance was tested in a repeated measures study of twenty drivers remotely teleoperating a modified utility vehicle through an obstacle field. Experimental results were analyzed with a one-way analysis of variance (ANOVA) and a significance threshold $p = 0.05$.

A. Setup

Experimental testing was performed on a four-wheeled, Kawasaki 4010 Mule utility vehicle fitted with steering and braking actuators, Velodyne LIDAR, NavCom GPS, a triaxial Inertial Measurement Unit (IMU), and a progressive area scan color CCD camera. An onboard Linux PC processed sensing data, ran controller code and transmitted video and other data to a teleoperator control station over an 802.11g wireless link. At the remote control station, human operators received video and state feedback

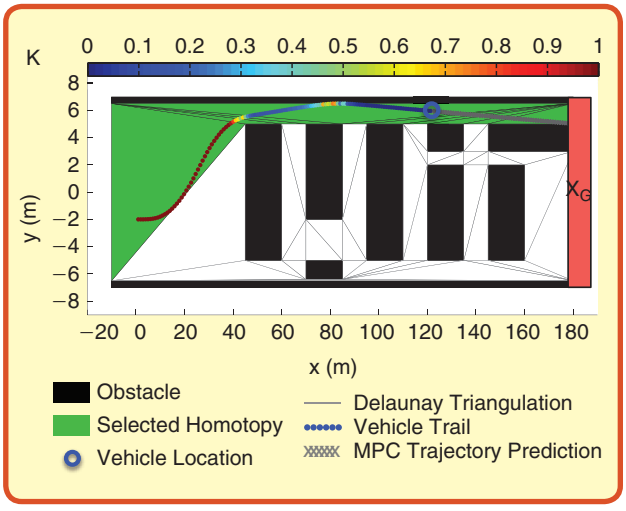

FIG 7 Simulation results demonstrating constraint-based semi-autonomous control through an obstacle field.

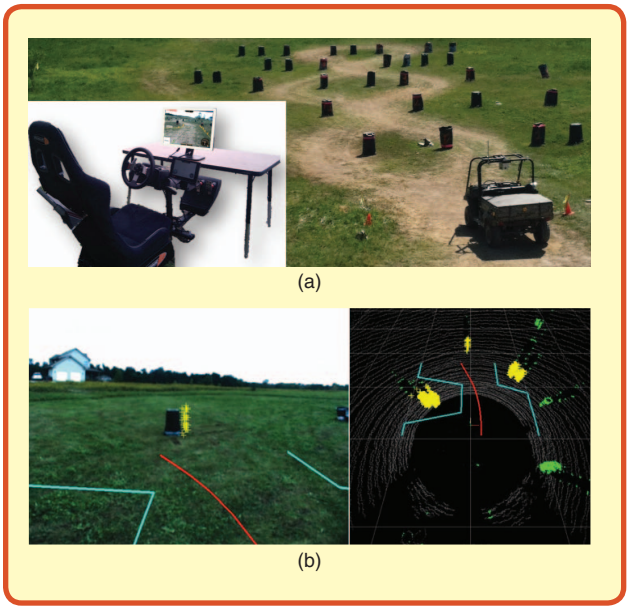

FIG 8 Experimental setup (a), constraints (cyan) and MPC prediction (red) on video and LIDAR feed (b).

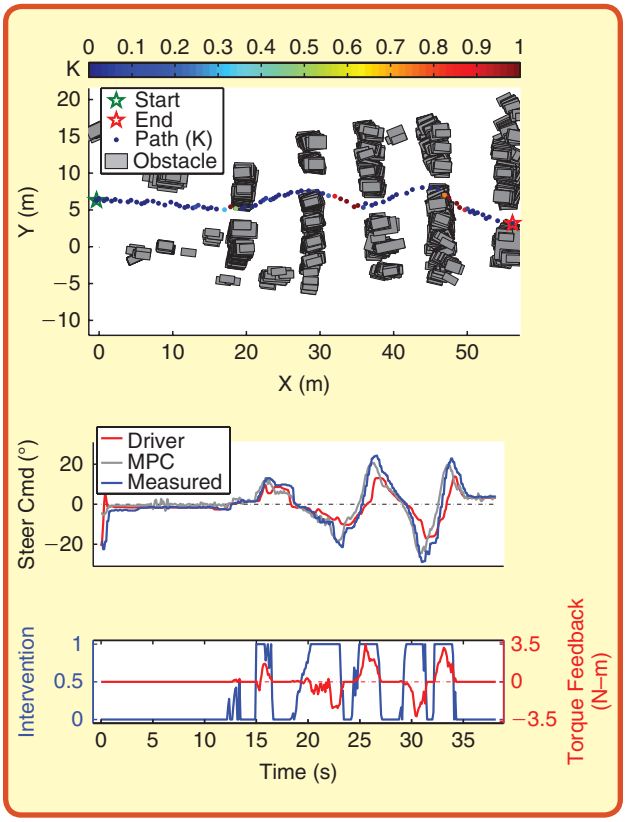

FIG 9 Plot of a typical run showing levels of intervention and its effect on the vehicle steering angle and the feedback provided to the operator.

data on a computer monitor and issued steering commands through a Logitech G27 steering wheel. Torque constraints were applied to the steering wheel via its dual-motor force feedback mechanism capable of applying 0–3.1 N-m of torque in either direction. Large barrels were arranged on a 50 m × 30 m field, and operators were instructed to navigate the course as quickly as possible without hitting them. In order to simulate periodic loss of vision caused by random occurrences such as camera obfuscation, sensor outages, and loss of communication, the camera feed seen by the teleoperator was blanked at random intervals for up to 2 seconds at a time.

Twenty operators, ranging in age from 20 to 51 years, with 0–35 years of driving experience, and 0 – 20 + years of video game experience were tasked with remotely (non-line-of-sight) teleoperating an unmanned ground vehicle across the 50-meter-long by 30-meter-wide obstacle course shown in Figure 8. In addition to this primary task, operators were asked to press a button on the steering wheel every time a warning indicator box in the lower left side of their screen indicated the need. To make this secondary task more challenging, the warning light took three values at random (~ 2-second) intervals during a trial: "Resting..." (white), "Don't Act!" (blue), and "Press Headlights!" (red). Users were instructed to press the button only when this indicator assumed its red, "Press Headlights!" state. Performance on this task was used to gauge differences in cognitive workload required by each control configuration (unassisted vs. assisted).

Prior to the tests, operators were briefed regarding the test setup, control interface, and semi-autonomy details. Each operator manually drove the vehicle through the course before the first round of testing began, and was given one warm-up run with each control configuration prior to each day of testing (first four trials not scored).

Altogether, 600 trials were conducted, with 480 of those trials scored (240 scored trials per test configuration). Each operator performed one round of testing per week for three weeks. Testing rounds consisted of 10 total trials (5 trials per configuration), with the configuration order randomized within each round to avoid ordering effects. Barrel placement on the obstacle course was changed between rounds to prevent users from relying on learned habits or worn paths to traverse the course. Following each round of testing, operators were administered an 8-question survey to gauge their acceptance of, comfort with, and confidence in each system configuration. Questions were posed on a 5-point Likert scale and included, "How easy was it to navigate the course without collisions," "How much control did you feel you had over the vehicle's behavior," "How fast did you feel comfortable traveling," and "How confident were you that the vehicle would do the right thing?"

Operators were instructed to minimize the performance "score", where **Score** = ***Time*** + 10***Collisions*** + 5***Brushes*** – ***Hits*** + ***Misses***. This score represents the total time it takes to navigate the course (in seconds), plus 10-second penalties for each collision, plus 5-second penalties for each "brush"

(barrel touched, but does not fall down), and 2-second penalties or rewards for incorrect/correct button presses in response to the secondary task. As an incentive for good performance, $150, $100, and $50 gift certificates were promised to the top three finishers.

B. Results

Figure 9 plots the results of a typical run with shared control and operator feedback enabled. Teleoperation performance was assessed from run data logged at 10 Hz. Dependent measures included collision frequency (collisions/run), course completion time (seconds), driver steer volatility (degrees), reaction time to the secondary task, and overall performance score (seconds).

Assessed over all drivers, courses, and dependent measures, constraint-based semi-autonomy improved teleoperational performance. With shared autonomy enabled, the number of collisions decreased by 78% ($F(1,478) = 37, p < 1e-8$) while average velocity increased by 26% ($F(1,478) = 86, p < 1e-18$), leading to a corresponding decrease in course completion time ($F(1,478) = 97, p < 1e-20$) and a 29% improvement in average driver score ($F(1,478) = 97, p < 1e-20$). Figure 10 plots the results of constraint-based semi-autonomy on six dependent measures of system performance.

With enough control intervention, similar improvements in collision avoidance and average speed might be expected of any controller. What makes this constraint-based framework unique is the minimal degree of adjustments it made to achieve the above results. Averaged across all drivers with shared control and feedback both enabled, the controller took only 43% of the available control authority ($\text{mean}(K) = 0.43, \text{SD} = 0.13$) to effect the above performance improvements. This minimal restriction on human commands afforded the operators significant freedom to maneuver as desired, leading 95% of operators to report feeling a *greater* sense of both confidence and control with assistance *enabled* than they felt when left to their own devices. This improvement in performance and confidence was accompanied by a significant decrease in driver steer volatility. With the semi-autonomous controller enabled, drivers were significantly more moderate in their control inputs—decreasing average steering volatility by 34%—from 14.5° to 9.5° ($F(1,478) = 147, p < 1e-27$).

Cognitively, enabling the semi-autonomous controller did not significantly affect the driver's ability to respond quickly to the secondary task. With the controller enabled, driver response times to the secondary task improved by an insignificant 3%—from 0.73 seconds (SD = 0.4) to 0.71 seconds (SD = 0.4) per alert. Considered in light of other performance improvements, this result suggests that any reduction in cognitive workload occasioned by the controller's offloading of high-threat tasks may have been nullified by a corresponding increase in visual and haptic cues

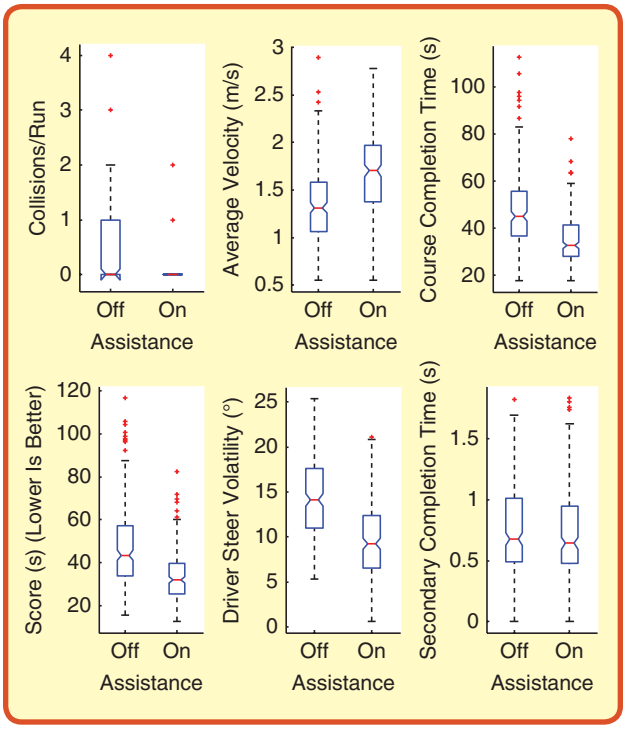

FIG 10 System performance relative to unassisted teleoperation.

that the operator had to process. In particular, the proximity of visual overlays to the warning indicator (see Figure 5) reduce the saliency of the latter, making changes in its state more difficult to notice.

VI. Conclusions

Semi-autonomous navigation requires planning and control methods capable of identifying desirable path homotopies and ensuring that the controlled system remains within them. This paper has illustrated one method for achieving minimally-restrictive, homotopy-based control through the planning and enforcement of constraints—rather than reference paths—on the states and control inputs of the vehicle. This method has been shown in simulation and experiment to improve human performance in the teleoperation task, eliminating 78% of collisions experienced by the unassisted teleoperator while simultaneously enabling a 26% increase in average speed. We note that the 0.096 collisions that continued to occur per trial were the result of the vehicle speed surpassing the capabilities of the steering actuators. This course was configured such that beyond a certain (operator-selected) trajectory and speed, it became impossible for the controller to turn the wheels fast enough to avoid collisions. We are currently extending the framework to include velocity constraints and corresponding acceleration intervention and expect this extension to eliminate 100% of avoidable collisions with minimal intervention.

Acknowledgment

The authors would like to thank Dan Rice, Kevin Melotti, Victor Perlin, Bryan Johnson, Rob Lupa, and Mitch Rohde for their assistance in setting up the Mule test vehicle and conducting experiments. This material is based on work supported by the US ARO under contract W911NF-11-1-0046 and DARPA DSO under the M3 program.

About the Authors

Sterling J. Anderson is a principal and co-founder of Gimlet Systems. He holds a BS from Brigham Young University and an M.S. and Ph.D. from MIT, where he was a National Defense Science and Engineering Graduate Fellow. His graduate research and post-graduate career have focused on shared control of human-machine systems. The methods described in this paper are one outgrowth of this research.

Sisir B. Karumanchi is currently a Postdoc at the Massachusetts Institute of Technology. He is working with Dr. Karl Iagnemma in the Robotic Mobility Group. He received a Bachelors degree in Mechatronic Engineering from the University of Sydney in 2005, and completed his Ph.D. with the Australian Centre for Field Robotics at the University of Sydney in 2010. His research interests include guaranteed safety for mobile robots in harsh off-road environments, semi-autonomous control, efficient simulation of vehicle-terrain interactions, and Bayesian non-parametric inference.

Karl Iagnemma is a Principal Research Scientist in the Mechanical Engineering Department at the MIT. He holds a BS from the University of Michigan, and an M.S. and Ph.D. from MIT, where he was a National Science Foundation Graduate Fellow. He has performed postdoctoral research at MIT, and has been a Visiting Researcher at the NASA Jet Propulsion Laboratory and the National Technical University of Athens (Greece). His primary research interests are in the areas of design, sensing, motion planning, and control of mobile robots in outdoor terrain, including modeling and analysis of robot-terrain interaction.

James M. Walker is a Software Engineer at Quantum Signal LLC specializing in robots and human-computer interaction. He holds a B.S. from the University of Michigan.

References

[1] National Highway Traffic Safety Administration, "2010 motor vehicle crashes: Overview," U.S. Dept. Transp., Washington, DC, Tech. Rep. DOT HS 811 552, Feb. 2012.

[2] Defense Manpower Data Center, "Military casualty information: Global war on terrorism," Statistical Information Analysis Division, Data, Analysis, and Programs Division, Jan. 2012.

[3] C. E. Lathan and M. Tracey, "The effects of operator spatial perception and sensory feedback on human-robot teleoperation performance," *Presence*, vol. 11, no. 4, pp. 368–377, 2002.

[4] J. Carlson and R. R. Murphy, "How UGVs physically fail in the field," *IEEE Trans. Robot.*, vol. 21, no. 3, pp. 423–437, 2005.

[5] P. M. Fitts, M. S. Viteles, N. L. Barr, D. R. Brimhall, and G. Finch, "Human engineering for an effective air-navigation and traffic-control system, and appendixes 1 THRU 3," Res. Foundation, Ohio State Univ., Columbus, OH, Tech. Rep., Mar. 1951.

[6] T. B. Sheridan and R. Parasuraman, "Human-automation interaction," *Rev. Hum. Factors Ergonomics*, vol. 1, no. 1, pp. 89–129, June 2005.

[7] J. Leonard, J. How, S. Teller, M. Berger, S. Campbell, G. Fiore, L. Fletcher, E. Frazzoli, A. Huang, S. Karaman, O. Koch, Y. Kuwata, D. Moore, E. Olson, S. Peters, J. Teo, R. Truax, M. Walter, D. Barrett, A. Epstein, K. Mahelona, K. Moyer, T. Jones, R. Buckley, M. Antone, R. Galejs, S. Krishnamurthy, and J. Williams, "A perception-driven autonomous urban vehicle," *J. Field Robot.*, vol. 25, no. 10, pp. 727–774, 2008.

[8] R. Vaidyanathan, C. Hocaoglu, T. S. Prince, and R. D. Quinn, "Evolutionary path planning for autonomous air vehicles using multiresolution path representation," in *Proc. Int. Conf. Intelligent Robots Systems*, Maui, HI, 2001, vol. 1, pp. 69–76.

[9] E. J. Rossetter and J. C. Gardes, "Lyapunov based performance guarantees for the potential field lane-keeping assistance system," *J. Dyn. Syst. Meas. Control Trans.*, vol. 128, no. 3, pp. 510–522, 2006.

[10] D. K. Cho and M. J. Chung, "Intelligent motion control strategy for a mobile robot in the presence of moving obstacles," in *Proc. IROS '91 IEEE/RSJ Int. Workshop Intelligent Robots Systems '91 Intelligence Mechanical Systems*, New York, 3–5 Nov. 1991, pp. 541–546.

[11] Y. Kuwata, S. Karaman, J. Teo, E. Frazzoli, J. P. How, and G. Fiore, "Real-time motion planning with applications to autonomous urban driving," *IEEE Trans. Control Syst. Technol.*, vol. 17, no. 5, pp. 1105–1118, Sept. 2009.

[12] H.-B. Yu and L. Gao, "Two-degree-of-freedom vehicle steering controllers design based on four-wheel-steering-by-wire," *Int. J. Vehicle Autono. Syst.*, vol. 5, nos. 1–2, pp. 47–78, 2007.

[13] J. Jansson, "Collision avoidance theory with application to automotive collision mitigation," Ph.D. dissertation, Dept. Elect. Eng., Linkoping Univ., Linköping, Sweden, 2005.

[14] J. Pohl, W. Birk, and L. Westervall, "A driver-distraction-based lane-keeping assistance system," in *Proc. Inst. Mech. Engineers Part I: J. Syst. Control Eng.*, vol. 221, no. 4, pp. 541–552, 2007.

[15] R. Mobus and Z. Zomotor, "Constrained optimal control for lateral vehicle guidance," in *Proc. IEEE Intelligent Vehicles Symp.*, Piscataway, NJ, 6–8 June 2005, pp. 429–434.

[16] T. Pilutti, G. Ulsoy, and D. Hrovat, "Vehicle steering intervention through differential braking," in *Proc. American Control Conf.*, Seattle, WA, 1995, vol. 3, pp. 1667–1671.

[17] A. Alleyne, "A comparison of alternative obstacle avoidance strategies for vehicle control," *Veh. Syst. Dyn.*, vol. 27, nos. 5–6, pp. 371–392, June 1997.

[18] T. Sattel and T. Brandt, "From robotics to automotive: Lane-keeping and collision avoidance based on elastic bands," *Veh. Syst. Dyn.*, vol. 46, no. 7, pp. 597–619, July 2008.

[19] A. Vahidi and A. Eskandarian, "Research advances in intelligent collision avoidance and adaptive cruise control," *IEEE Trans. Intell. Transp. Syst.*, vol. 4, no. 3, pp. 143–153, Sept. 2003.

[20] J. J. Gibson and L. E. Crooks, "A theoretical field-analysis of automobile-driving," *Amer. J. Psychol.*, vol. 51, no. 3, pp. 453–471, July 1938.

[21] T. C. Biedl, E. D. Demaine, S. Lazard, S. M. Robbins, M. A. Soss, A. Aggarwal, and C. P. Rangan, "Convexifying monotone polygons," in *Proc. 10th Int. Symp. Algorithms Computation*, 1999, pp. 415–424.

[22] W. Lenhart and S. Whitesides, "Reconfiguring closed polygonal chains in Euclidean d-space," *Discrete Comput. Geometry*, vol. 13, no. 1, pp. 123–140, 1995.

[23] D. Fox, W. Burgard, and S. Thrun, "The dynamic window approach to collision avoidance," *IEEE Robot. Autom. Mag.*, vol. 4, no. 1, pp. 23–33, Mar. 1997.

[24] S. J. Anderson, S. C. Peters, T. E. Pilutti, and K. Iagnemma, "An optimal-control-based framework for trajectory planning, threat assessment, and semi-autonomous control of passenger vehicles in hazard avoidance scenarios," *Int. J. Veh. Auton. Syst.*, vol. 8, nos. 2–4, pp. 190–216, 2010.

ITS